Proceedings of the 17th International Heat Transfer Conference, IHTC-17
14 – 18 August 2023, Cape Town, South Africa

IHTC-17 | ID: 158

# MEASUREMENT OF NEAR-WALL LIQUID TEMPERATURE BASED ON TOTAL INTERNAL REFLECTION FLUORESCENCE MICROSCOPY

**R. Kuriyama[1*], K. Ueda[1], K. Tatsumi[1] and K. Nakabe[1]**

[1] Kyoto University, Kyotodaiagku-katsura, Nishikyo-ku, Kyoto 615-8540, Japan

## ABSTRACT

For the development of a measurement technique for near-wall liquid temperature, the present study proposes two methods based on total internal reflection fluorescence microscopy (TIRFM). One is based on two-color laser induced fluorescence (LIF) which exploits the temperature dependence of the intensity ratio of two fluorescence bands from a single fluorescent dye. The other is based on fluorescence polarization (FP) which exploits the depolarization phenomenon due to the rotational Brownian motion of fluorescent molecules. In these methods, evanescent wave was generated at the interface between glass wall and solution in a microchannel, so that only the fluorescent molecules near the wall within ~100 nm were excited. In two-color LIF method using sulforhodamine B (SrB), the calibration result showed that the fluorescence intensity ratio of 580–590 nm to 612–644 nm decreased with temperature in the range of 25–40 °C. However, the intensity ratio also decreased with time, which is presumably caused by the adsorption of SrB to the glass wall. In FP method using uranine, polarization degree decreased with temperature in the range of 25–40 °C with the sensitivity of 0.7%/°C, which agrees with the theoretical value qualitatively. Temperature distribution measurement was also conducted using FP method in the vicinity of the channel bottom wall on which an Au line heater of 200 nm thick and 20 μm wide was patterned. The measured and calculated temperature distributions of the near-wall liquid agreed well within 1°C in the area more than 50 μm away from the heater in the spanwise direction.

**KEY WORDS:** Liquid temperature measurement, Near-wall region, Evanescent field, Two-color LIF, Fluorescence polarization

## 1. INTRODUCTION

Thin liquid layer at the solid-liquid interface plays a crucial role in heat transfer phenomena both in single-phase and two-phase flows. In single-phase liquid flow in micro- and nanochannels, for example, the no-slip thermal boundary condition may fail due to the scale effect. This results in the temperature jump at the boundary of liquid and the heating surface, which has significant effect on the heat transfer characteristics as the channel scale decreases [1,2]. In gas-liquid two-phase flow, the dynamics of a thin annular liquid film which is driven by forced gas or vapor flow attract interest for efficient thermal management with high heat flux [3,4]. The temperature gradient in liquid-gas interface generates thermocapillary force which induces convection and rupture of the film. Also in nuclear boiling, evaporation of a thin liquid film called microlayer, which is formed under a bubble growing on a heating surface, is directly related to the bubble growth or shrinkage [5,6]. For understanding and controlling these complicated heat transfer phenomena, advanced experimental techniques have been applied to the solid-liquid interface. For investigating thermal slip length at the interface, time-domain thermoreflectance [1,7] has been used to obtain thermal conductance of the interface. Surface-mounted MEMS sensors [8,9] and IR thermography [10,11] have been employed as powerful tools for heat transfer measurements in boiling phenomena. However, it is still difficult to directly visualize two-dimensional temperature distribution in liquid layer with submicron spatial resolution.

*Corresponding Author: kuriyama.reiko.2m@kyoto-u.ac.jp

For an alternative approach, total internal reflection fluorescence microscopy (TIRFM) which utilizes evanescent field can be a candidate for a surface-specific and non-contact observation with high spatial resolution. Although the most common applications of TIRFM are in cell biology and biochemistry, TIRFM can also be applied to the diagnostics of thermal flow fields [12-14]. Guasto et al. [13] measured liquid temperature in the region within 200 nm from a microchannel wall by using temperature sensitive CdSe/ZnS quantum dots excited by evanescent field. They employed a ratiometric thermometry using a temperature-insensitive rhodamine 110 dye to compensate the spatial distribution of the illumination and realized an accuracy of ±4.9 ºC. Kim and Yoda [14] performed temperature measurements within 300 nm from the channel wall using evanescent field and a temperature-sensitive fluorophore (fluorescein). They used an indium tin oxide film heater deposited on the bottom wall of the minichannel to generate temperature gradients and the measurement results were in good agreement with the numerical simulation within 0.65 ºC. Although the influence of using dye/quantum dots on the surface properties (such as interfacial tension) requires careful consideration, these TIRFM-based techniques are expected to have high potential to analyse various near-wall heat transfer phenomena.

In the present study, we propose two imaging techniques for near-wall liquid temperature based on TIRFM. One is based on two-color laser induced fluorescence (LIF) which exploits the temperature dependence of the intensity ratio of two fluorescence bands from a single fluorescent dye. The other is based on fluorescence polarization (FP) which exploits the depolarization phenomenon due to the rotational Brownian motion of fluorescent molecules. These methods determine the temperature by ratiometric procedure based on intensity ratio or polarization degree which is normalized by the total fluorescence intensity. Therefore, it is expected that the methods are robust to spatio-temporal variation in fluorescence intensity caused by various factors such as variations of excitation intensity and fluorophore concentration, and fluorescence degradation. This paper experimentally investigates the temperature dependences of the intensity ratio and polarization degree of the fluorescence induced by evanescent field to examine the feasibility of the proposed methods. We also tried to visualize liquid temperature distribution in the vicinity of the channel wall on which a line heater of 200 nm thick and 20 μm wide was patterned to generate temperature gradient.

## 2. MEASUREMENT PRINCIPLE

**2.1 Total internal reflection fluorescence microscopy (TIRFM)** TIRFM is an optical technique which enables excitation of fluorescent molecules only in the vicinity of an interface by using evanescent field. When light passes from one medium (with higher refractive index, $n_1$) to another (with lower refractive index, $n_2$ ($< n_1$)), some is reflected and the other is transmitted into the second medium. If the incident angle $\theta_i$ is larger than the critical angle $\theta_c$ (= $\sin^{-1}(n_2/n_1)$), all the light is reflected, i.e., it undergoes total internal reflection. Even in this case, the electric field penetrates through the interface and propagates parallel to the surface (in Fig. 1). This field is termed evanescent field. The intensity of evanescent wave $I_e(z)$ decays exponentially with the distance, $z$, from the interface as [15]:

$$I_e(z) = I_e(0)\exp\left(-z/z_p\right), \tag{1}$$

where

$$z_p = \lambda_i \Big/ 4\pi\sqrt{n_1^2 \sin^2\theta_i - n_2^2}\ . \tag{2}$$

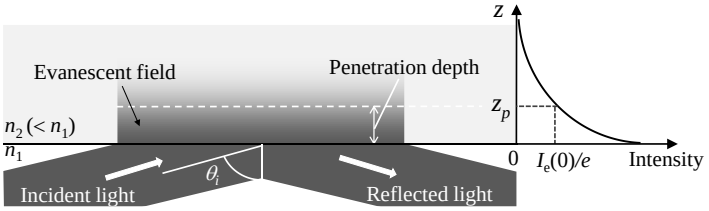


**Fig. 1** Generation of evanescent field and its intensity distribution.

$I_e(0)$ represents the intensity at the interface ($z = 0$). The characteristic length, $z_p$, is called the penetration depth and $\lambda_i$ is the wavelength of the incident light in vacuum. Since $z_p$ is generally on the order of $\lambda_i$ or smaller, the evanescent field can selectively illuminate the near-wall area within ~100 nm from the interface.

**2.2 Two-color laser induced fluorescence (two-color LIF)** LIF is often used to determine two-dimensional distribution of scalar quantity (such as temperature, concentration, for example) based on the dependence of fluorescence intensity on these quantities. The fluorescence intensity observed at a wavelength $\lambda$ can be expressed as [16]:

$$I_f(\lambda,T) = A(\lambda) I_0 C_f \phi(\lambda,T) \varepsilon L, \tag{3}$$

where $A$ is the collection efficiency of the detection system, $I_0$ is the intensity of the excitation light, $C_f$ is the concentration of the fluorescent molecule, $\phi$ is the quantum yield, $\varepsilon$ is the molar absorption coefficient, and $L$ is the length along the optical path of the excitation light. The quantum yield $\phi$ is temperature dependent in most organic fluorescent molecules, whereas $\varepsilon$ does not have significant temperature dependence. As a result, the fluorescence intensity changes with temperature, which has the sensitivity typically on the order of 1%/ºC [17]. Based on this principle, the fluid temperature measurement can be realized by measuring the fluorescence intensity. However, as seen from Eq. (3), the fluorescence intensity $I_f$ is affected by various factors as well as temperature. Generally, excitation intensity $I_0$ and the concentration of fluorescent molecule $C_f$ are not uniform over the measurement area and can temporally fluctuate. To avoid the influence of these factors on the temperature measurement, two-color LIF, which exploits the intensity ratio of two fluorescence bands from a single fluorescent dye, is promising. If the two fluorescence bands with different temperature dependences are spectrally separated and simultaneously detected by two cameras, the ratio of the detected intensities, $R_f$, can be defined as follows:

$$R_f = \frac{I_{f1}(T)}{I_{f2}(T)} \approx \frac{A_1 \phi_1(T)}{A_2 \phi_2(T)}, \tag{4}$$

where $I_{f1}$ and $I_{f2}$ is the fluorescence intensities of the wavelength bands with high and low (or opposite) temperature sensitivities, respectively. The intensity ratio $R_f$ is independent of $I_0$ and $C_f$, but it depends on $T$ through the ratio of the quantum efficiencies at two wavelength bands.

**2.3 Fluorescence polarization (FP)** When randomly oriented fluorescent molecules are irradiated by a linearly-polarized excitation light, the probability of the absorption is proportional to the value $\cos^2\theta$, where $\theta$ is the angle between the directions of excitation polarization and absorption moment of the molecules. If the excited molecules are at stationary state, they emit the fluorescence polarized in the same direction with the absorption moment. On the other hand, if the excited molecules are suspended in fluid, they experience rotational Brownian motion during the fluorescence lifetime. Consequently, the emission moments, which are parallel to the absorption moments, are randomized according to the extent of their rotation. Depolarization of fluorescence is therefore observed with the degree which is related to the fluid temperature, viscosity, and the molecular size.

Polarization degree, $P$, is defined as a function of $I_{\parallel}$ and $I_{\perp}$, which are the fluorescence intensities of the components that are parallel and perpendicular to the excitation polarization, respectively:

$$P = \frac{I_{\parallel} - I_{\perp}}{I_{\parallel} + I_{\perp}}. \tag{5}$$

Since $P$ is normalized by the total fluorescence intensity and follows the rotational motion of the molecules only, FP measurement is less influenced by the spatio-temporal fluctuation of $I_0$, $C_f$, and $\phi$, compared to LIF measurement. Perrin [18] theoretically derived the equation which relates $P$ to the fluorescence lifetime $\tau$ and the rotational diffusion of fluorescent molecules as:

$$(\frac{1}{P} - \frac{1}{3}) = (\frac{1}{P_0} - \frac{1}{3})(1 + \frac{k_B T}{\mu V}\tau), \tag{6}$$

where $P_0$ is the intrinsic polarization defined as the polarization degree of the molecule at stationary state (in absent of rotation), $k_B$ is the Boltzmann constant, and $V$ is the hydrodynamic volume of the fluorescent molecule. $T$ and $\mu$ are the absolute temperature and viscosity of the fluid, respectively. From Eq. (6), the reciprocal of $P$ shows a linear relation with $T/\mu$, if $V$ and $\tau$ remains constant during the measurement. In the present study, FP measurement was conducted by using evanescent field illumination generated with laser beam polarized perpendicular to the incident plane (i.e., *s*-polarized).

## 3. EXPERIMENTAL SECTION

**3.1 Experimental setup** Fig. 2 shows a schematic of the experimental setup for TIRFM-based temperature measurements. A continuous wave laser (Coherent; Genesis MX488-1000SLM) operating at 488 nm was used to generate evanescent field. The laser beam was introduced horizontally into a trapezoidal prism ($n$ = 1.522) mounted on a temperature control stage equipped with Peltier devices. The beam travelled into a glass slide (silica, $n$ = 1.463 or TEMPAX, $n$ = 1.477) which serves as the bottom wall of a microchannel. An immersion oil ($n$ = 1.518) was used between the prepared slide and the prism to optically couple them. The beam underwent total internal reflection at the interface between the glass and the solution in the microchannel and generated the evanescent field. The incident angle of the total internal reflection was 79 or 83º (depending on the glass material) and the penetration depth was estimated to be ~70 nm from Eq. (2). The area where the evanescent field was generated had an ellipsoidal shape with Gaussian intensity profile and the lengths of the major and minor axes of the area were 5.3 mm and 1.2 mm, respectively.

The fluorescence was collected by an objective lens (Olympus; 10x, NA=0.25 in two-color LIF, 20x, NA=0.40 in FP), split into two components ($I_{f1}$ and $I_{f2}$ in two-color LIF, $I_{\parallel}$ and $I_{\perp}$ in FP), and measured by two sCMOS cameras (Andor; Zyla 4.2 PLUS, 2048×2048 pixels, 16bit) simultaneously. The pixel resolution of the images was 0.65 μm/pixel in two-color LIF and 0.33 μm/pixel in FP, respectively. In two-color LIF measurement, a dichroic mirror (Semrock; FF506-Di03) and fluorescence filters (Semrock; FF01-628/32-25 and FF01-585/11-25) were used to spectrally separate the components. On the other hand, in FP measurement, a bandpass filter (Chroma; AT535/40m) was used to extract the fluorescence and a polarizing beam splitter (Thorlabs; PBS251) was used to split the two polarizing components.

**3.2 Solution and microchannel** In two-color LIF measurement, sulforhodamine B (Tokyo Chemical Industry; A0600, SrB) was dissolved in a buffer solution of $7.0\times10^{-3}$ mol/L sodium tetraborate (pH 9.2) to suppress the adsorption to glass wall [19]. The concentration of SrB was set at $5.0 \times 10^{-5}$ mol/L. When excited by 488 nm, the fluorescence intensity of SrB decreases with temperature at 580−590 nm,

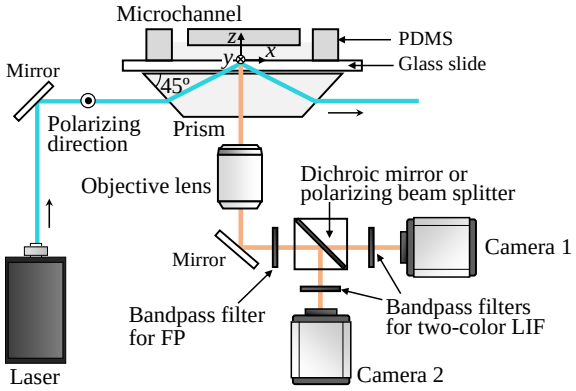


**Fig. 2** Schematic of the experimental setup for TIRFM-based temperature measurements.

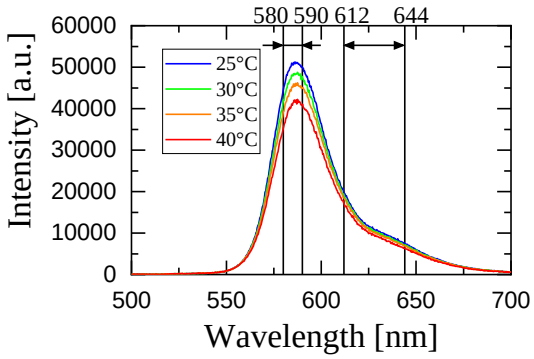


**Fig. 3** Fluorescence spectra of SrB solution at different temperature conditions.

but it shows little change at 612–644 nm as shown in Fig. 3. Thus, the fluorescence filters which transmit these wavelength ranges were selected. The fluorescence measured through these filters were treated as $I_{f1}$ and $I_{f2}$ in Eq. (4), respectively. In FP measurement, uranine (Nacalai Tesque, #3581692) was dissolved in a buffer solution of $7.0\times10^{-3}$ mol/L sodium tetraborate at the concentration of $1.0\times10^{-4}$ mol/L to obtain sufficient fluorescence intensity without suffering from concentration depolarization.

Fluorescent dye solution was supplied to a microchannel at a constant flow rate using a syringe pump (Nihon Koden; CFV-3200). As shown in Fig. 2, the microchannel was comprised of polydimethyl siloxane (PDMS) chip and a glass slide. The channel structure (width: 3 mm, height: 44 μm) was molded in a PDMS layer by soft lithography, and bonded to the glass slide by oxygen-plasma treatment. For FP measurement, the glass surface was changed to be hydrophobic by silane coupling treatment using commercially available glass coating agent (PPG; Aquapel) to minimize the adhesion of fluorescent molecules. To monitor the channel bottom temperature, K-type thermocouples of 100 μm in diameter were inserted in 1-mm diameter holes of PDMS chip.

**3.3 Experimental conditions** The laser power at the measurement area (i.e., the glass-solution interface in the microchannel) was estimated to be 160 mW based on the power measured just before entering the prism and the reflection rate at the prism surface. The temperature of channel bottom wall was controlled in the range 25–40 °C using the temperature control stage. The exposure time was set at 0.5 s in two-color LIF and 1.0 s in FP measurement, respectively. In both measurements, a pair of 100 successive images were obtained by two cameras. The averaged images of different color/polarization components were registered to one another by using the affine transformation matrix which was obtained by camera calibration. Then the distributions of fluorescence intensity ratio $R_f$ or polarization degree $P$ were calculated using Eq. (4) or Eq. (6). It should be noted that the degradation (or fading) of the fluorescence on the fluorescence intensity measurement was negligible, since these measurements were conducted in the presence of flow.

## 4. RESULTS AND DISCUSSION

### 4.1 Relationship between temperature and intensity ratio by two-color LIF measurement

Fig. 4 shows the result of three measurements. The temperature was increased from 25 °C to 40 °C with 5 °C-increments and then decreased to 25 °C with 5 °C-decrements. The time and spatial averaged values of the intensity ratio in the measurement area (1268 μm × 585 μm) are plotted against the temperature with the neighboring number showing the measurement order. Although the intensity ratio decreased with temperature as expected from the fluorescence spectra in Fig. 3, the temperature sensitivity was higher when the temperature was increased (plot points #1–#4) compared with the sensitivity when the temperature was decreased (plot points #4–#7). When comparing the values at the same temperature (plot points #1 and #7, for example), the intensity ratio measured later shows lower value by approximately 5%. This trend can be observed in all three measurements in Fig. 4 and seems related to the temporal change of fluorescence spectra. Fig. 5(a) shows the time variation of the intensity ratio measured at constant temperature condition. The intensity ratio monotonically decreased with time by 5% per hour and this is presumably caused by dye adsorption to channel wall. Fig. 5(b) shows the comparison of the fluorescence spectrum of SrB solution flowing in microchannel (black line) and that of SrB adsorped to the glass wall (red line). The peak wavelengths of these spectra are 588 nm and 581 nm, respectively, i.e., the spectrum of adsorbed SrB is slightly blue shifted compared that of solution. This leads to the decrease in fluorescence intensity ratio with progression of dye adsorption over time and complicates the temperature calibration. Also in the previous report by Kim and Yoda [14], where they at first intended to measure near-wall liquid temperature by two-color approach using fluorescein and SrB, the adsorptive characteristics of SrB prevented them from using it in the end. From these results, it is suggested that some surface treatment should be employed to avoid adsorption when using SrB in TIRFM-based measurement.

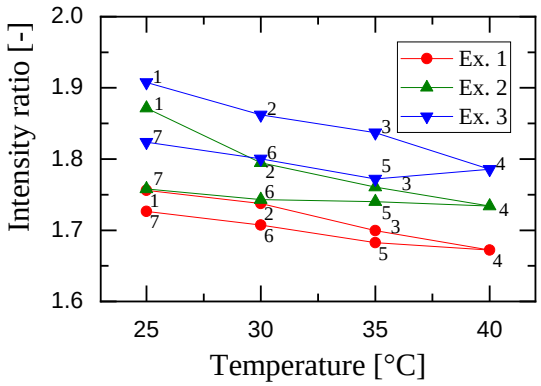


**Fig. 4** Relationship between temperature and the intensity ratio of fluorescence in 580–590 nm to 612–644 nm nm from SrB solution obtained by two-color LIF measurement.

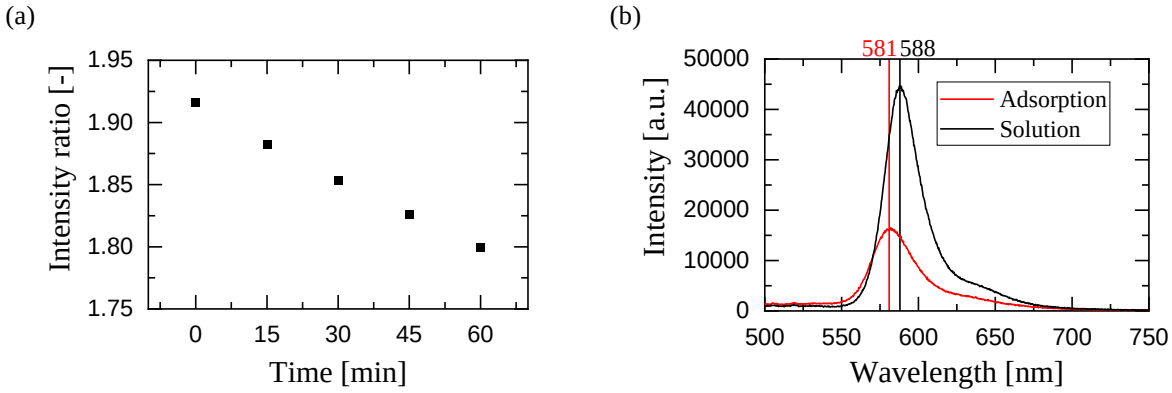


**Fig. 5** (a) Temporal change in the fluorescence intensity ratio and (b) comparison of fluorescence spectra from SrB in solution and in absorbed state.

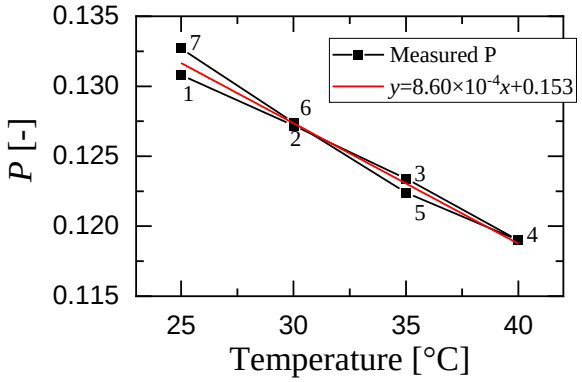


**Fig. 6** Relationship between temperature and the fluorescence polarization degree *P* from uranine solution obtained by FP measurement.

**4.2 Relationship between temperature and polarization degree by FP measurement** Fig. 6 shows the measurement result obtained by FP method in the same manner as the previous section. The plot point represents the time and spatial averaged polarization degree in the measurement area (520 μm × 325 μm) and the neighboring number shows the measurement order. The polarization degree *P* decreased with temperature monotonically, which agrees with the theoretical prediction in Eq. (6). The difference in the measured *P* value at the same temperature condition was within approximately 1%, which was much smaller than the difference observed in two-color LIF measurement. The temperature sensitivity of *P* was 0.7%/ºC, which was evaluated from the slope of the red straight line in Fig. 6 derived by the least squares regression. The theoretical *P* values calculated for 25 and 40 °C based on Eq. (6) are 0.017 and 0.012, respectively. There is large offset in the absolute values between theoretical and measured *P* values, which is mainly attributed to the transmission characteristics of the optical elements such as dichroic mirror. The theoretical decrease of *P* between 25–40 °C is, however, on the same order compared with the measured value, which supports the validity of the measurement result.

**4.3 Temperature distribution measurement by FP method** For the validation of TIRFM-based FP method, two-dimensional temperature distribution measurement was conducted in the near-wall region of the straight microchannel where a temperature gradient was formed in the spanwise direction by using an Au line heater. The width and height of the channel were 1 mm and 50 μm, respectively, and the uranine solution was supplied at the constant flow rate of 3 μL/min. The heater was patterned on the surface of the glass slide along the longitudinal center line of the channel (i.e., patterned on the channel bottom wall along the flow direction). The thickness, width and length of the heater were 200 nm, 20 μm, and 15 mm, respectively, and the resistance was 137 Ω at room temperature. The microchannel was set on the prism mounted on the temperature control stage. The field of view (650 × 650 μm$^2$) was set at the center of the channel in the spanwise and the streamwise directions. The experiment was conducted in the following procedure. First, calibration experiment was conducted in the microchannel in the same way as the previous section using the temperature control stage. Then the temperature control stage was switched off and constant current of 40 mA was supplied to the heater. The polarization measurement was conducted after the temperature reached steady state.

Fig. 7 shows the measurement result. The near-wall temperature distribution around the heater (shown in gray color) was clearly visualized. Although a fringe pattern aligned along the *x*-direction can be observed, the fluid temperature is higher near the heater and gradually decreases with distance in the spanwise direction due to the thermal diffusion. The measured temperature seems almost constant along the *x*-direction. These trends qualitatively agrees with the temperature distribution obtained by the numerical simulation (not shown here). In the calculated distribution, large temperature gradient was observed around the heater in the spanwise direction, whereas the temperature increase along the flow direction was within 0.1 °C in -300 μm < *x* < 300 μm. For quantitative comparison, Fig. 8 shows the

spanwise distributions of the measured and calculated temperatures. The measured distribution in Fig. 7 was averaged over the *x*-direction and compared with the calculated distribution at *x* and *z* =0. These two distributions agree within 1 °C in the areas -50 μm ≥ *y* and *y* ≥ 50 μm, but the measured temperature is lower than the calculated one by 5 °C in maximum in the areas $|y| \leq 50$ μm. In addition, the temperature profile is somewhat asymmetric about the *y* axis and shows lower value in the area $y < 0$ μm, which might be caused by the misalignment of the Au line heater, i.e., the heater was not aligned perfectly parallel to the flow direction. Although the exact causes of the fringe pattern and the large temperature difference near the heater have not been understood yet, the above results indicate the potential of TIRFM-based FP method for two-dimensional measurement of near-wall liquid temperature in channel flow. We will further conduct experiments to examine the above issues and improve measurement accuracy.

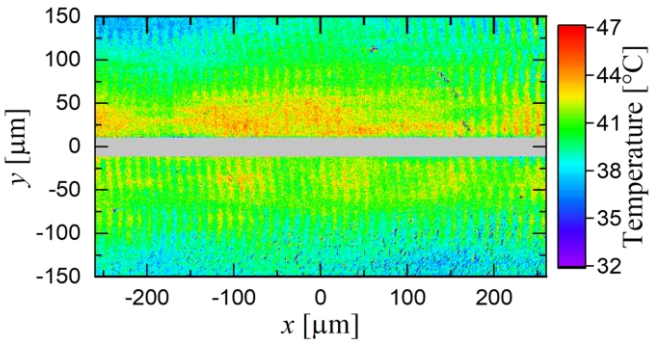


**Fig. 7** Near-wall temperature distribution around the Au line heater (shown in gray color) measured by FP measurement.

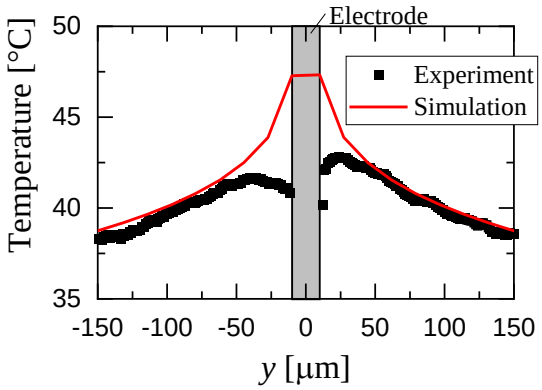


**Fig. 8** Comparison of spanwise near-wall temperature distributions obtained by FP measurement and numerical calculation.

## 6. CONCLUSIONS

The present study proposed TIRFM-based two-color LIF and FP for measurement of liquid temperature in the near-wall region and investigated the feasibility of these methods by measuring the temperature dependences of the intensity ratio and polarization degree of the fluorescence induced by evanescent field. In two-color LIF measurement using SrB, the fluorescence intensity ratio of 580–590 nm to 612–644 nm bands decreased with time by SrB adsorption to channel wall, as well as with temperature, which made the calibration difficult. In FP measurement using uranine, the polarization degree decreased with temperature in the range of 25–40 °C with the sensitivity of 0.7%/ºC. Using FP method, non-uniform near-wall temperature field was visualized in the microchannel equipped with a line heater. The measurement results agreed well with the numerical simulation within 1 ºC in the area more than 50 μm away from the heater in the spanwise direction. We will further conduct temperature calibration and distribution measurement to examine the measurement reliability and try to apply this method for the measurement near three-phase contact line or in gas-liquid two phase flow in future work.

## ACKNOWLEDGMENT

This work was partially supported by the Japan Society for the Promotion of Science KAKENHI, Grant-in-Aid for Early-Career Scientists Grant Number 21K14095.

## NOMENCLATURE

| | | | | | |
|---|---|---|---|---|---|
| $A$ | collection efficiency of system | [-] | $T$ | Absolute temperature | [K] |
| $C_f$ | concentration of fluorescent molecule | [mol/L] | $V$ | Hydrodynamic volume | [$m^3$] |
| $k_B$ | Boltzmann constant | [J/K] | $x$ | Cartesian axis distance | [m] |
| $L$ | Length along optical path | [m] | $y$ | Cartesian axis distance | [m] |
| $n$ | Refractive index | [-] | $z$ | Cartesian axis distance | [m] |
| $I$ | Light intensity | [W/$m^2$] | $z_p$ | Penetration depth | [m] |
| $I_e$ | Intensity of evanescent wave | [W/$m^2$] | $\varepsilon$ | Molar absorption coefficient | [L/(mol·m)] |
| $I_f$ | Fluorescence intensity | [W/$m^2$] | $\phi$ | Quantum yield | [-] |
| $I_0$ | Intensity of excitation light | [W/$m^2$] | $\lambda$ | Wavelength of light | [m] |
| $I_\parallel$, $I_\perp$ | Fluorescence intensity of component parallel/ perpendicular to excitation polarization | [W/$m^2$] | $\lambda_i$ | Wavelength of incident light in vacuum | [m] |
| | | | $\mu$ | Viscosoity | [Pa·s] |
| $P$ | Polarization degree | [-] | $\theta_i$ | Incident angle | [rad] |
| $P_0$ | Intrinsic polarization | [-] | $\tau$ | Fluorescence lifetime | [s] |
| $R_f$ | Fluorescence intensity ratio | [-] | | | |

## REFERENCES

[1] Ge, Z., Cahill D.G., and Braun P.V., "Thermal conductance of hydrophilic and hydrophobic interfaces," *Phys. Rev. Lett.*, Vol. 97, 186101, (2006).
[2] Nagayama, G., Matsumoto, T., Fukushima, K., and Tsuruta, T., "Scale sffect of slip boundary condition at solid –liquid interface," *Sci.Rep.*, Vol. 7, 43125, (2017).
[3] Kabov, O.A., Lyulin, Y.V., Marchuk, I.V., and Zaitsev, D.V., "Locally heated shear-driven liquid films in microchannels and minichannels," *Int. J. Heat Fluid Flow*, Vol. 28, pp. 103-112, (2007).
[4] Zaitsev, D.V. and Belosludtsev, V.V., "Experimental setup for studying two-phase flows in micro- and minichannels at ultra-high heat fluxes: methodology and first experimental results," *J. Phys.: Con. Ser.*, Vol. 2119, 012133, (2021).
[5] Moor, F.D. and Mesler, R.B., "Surface temperature fluctuations during nucleate boiling of water," *Am. Inst. Chem. Eng. J. (A.I.Ch.E. Journal)*, Vol. 7, No. 4, pp. 620-624, (1961).
[6] Cooper, M.G. and Lloyd, A.J., "The microlayer in nucleate pool boiling," *Int. J. Heat Mass Transf.*, Vol. 12, pp. 895-913, (1969).
[7] Costescu, R.M., Wall, M.A., and Cahill D.G., "Thermal conductance of epitaxial interfaces," *Phys. Rev. B*, Vol. 67, 054302, (2003).
[8] Yabuki, T. and Nakabeppu, O., "Heat transfer mechanisms in isolated bubble boiling of water observed with MEMS sensor," *Int. J. Heat Mass Transf.*, Vol. 76, pp. 286-297, (2014).
[9] Yabuki, T. and Nakabeppu, O., "Microscale wall heat transfer and bubble growth in single bubble subcooled boiling of water," *Int. J. Heat Mass Transf.*, Vol. 100, pp. 851-860, (2016).
[10] Gerardi, C., Buongiorno, J., Hu, L.-W., and McKrell, T., "Study of bubble growth in water pool boiling through synchronized, infrared thermometry and high-speed video," *Int. J. Heat Mass Transf.*, Vol. 53, pp. 4185-4192, (2010).
[11] Tanaka, T., Miyazaki, K., and Yabuki, T., "Observation of heat transfer mechanisms in saturated pool boiling of water by high-speed infrared thermometry," *Int. J. Heat Mass Transf.*, Vol. 170, 121006, (2021).
[12] Kazoe, Y. and Yoda, M., "Evanescent wave-based flow diagnostics," *J. Fluid Engineering*, Vol. 135, 021305 (2013).
[13] Guasto, J.S. and Breuer, K.S., "Simultaneous, ensemble-averaged measurement of near-wall temperature and velocity in steady micro-flows using single quantum dot tracking," *Exp. Fluids*, Vol. 45, pp.157-166, (2008).
[14] Kim, M. and Yoda, M., "Extending fluorescence thermometry to measuring wall surface temperatures using evanescent-wave illumination," *J. Heat Transfer*, Vol. 134, 011601, (2012).
[15] Axelrod, D., "Total internal reflection fluorescence microscopy in cell biology," *Traffic*, Vol. 2, pp. 764–774, (2001).
[16] Walker, D.A., "A fluorescence technique for measurement of concentration in mixing liquids," *J. Phys. E: Sci. Instr.*, Vol. 20, pp. 217–224, (1987).
[17] Sakakibara, J. and Adrian, R.J., "Whole field measurement of temperature in water using two-color laser induced fluorescence," *Exp. Fluids*, Vol. 26, pp. 7-15, (1999).
[18] Perrin, F., "La fluorescence des solutions. Induction moléculaire—polarisation et durée d'émission— photochimie," *Ann. Phys.*, Vol. 12, pp. 169–275, (1929).
[19] Kasnavia, T., Vu, D., and Sabatini, D.A., "Fluorescent dye and media properties affecting sorption and tracer selection," *Groundwater*, Vol. 37, No. 3, pp. 376-381, (1999).